(Received 13 March 2025, Accepted 14 May 2025, Scheduled 26 May 2025)

Half-Mode Substrate Integrated Waveguide Cavity Slot Antenna with Half-Octagonal Ring Slot at S-Band Frequency

Andri Setyawan[1], Dian Widi Astuti[1,*], Mudrik Alaydrus[1], Yuyu Wahyu[2], and Norbahiah Misran[3]

[1]*Department of Engineering, Universitas Mercu Buana, Jakarta 11650, Indonesia*
[2]*Research Centre for Electronics and Telecommunications, Indonesian Institute of Sciences, Bandung 40135, Indonesia*
[3]*Department of Electrical, Electronic & System Engineering, Faculty of Engineering and Built Environment Universiti Kebangsaan Malaysia, UKM Bangi, Selangor 43600, Malaysia*

ABSTRACT: This paper presents a design of a half-mode substrate integrated waveguide (HMSIW) antenna for S-band frequencies using half-octagonal ring slots to achieve significant bandwidth enhancement. The proposed structure integrates a half-octagonal ring slot within the HMSIW cavity to enhance impedance bandwidth by exciting dual resonant modes — TE_{101} and TE_{102}. The antenna achieves a measured fractional bandwidth (FBW) of 5.6%, corresponding to an operational range of 3.15 to 3.33 GHz, and a simulated FBW of 5.2% from 3.17 to 3.40 GHz. Compared to conventional cavity-backed SIW antennas, this configuration offers a 50% size reduction while maintaining stable gain between 3.1 dBi and 5.6 dBi and exhibiting a directional linear radiation pattern in the horizontal plane. The integration of dual-resonance excitation within a single compact HMSIW cavity represents a significant advancement in bandwidth enhancement for planar antennas. This design offers a feasible and efficient solution for modern wireless applications requiring miniaturized and compact size in S-band frequencies.

1. INTRODUCTION

Substrate integrated waveguide (SIW) antennas are planar antennas that utilize integrated dielectric and metallic via structures within standard printed circuit board (PCB) substrates to emulate waveguide characteristics and support guided electromagnetic wave propagation. SIW antennas offer advantages such as low cost, ease of fabrication, and compatibility with microwave planar circuits [1–3]. However, conventional SIW antennas often suffer from narrow impedance bandwidths, typically below 2%, which restricts their application in broadband systems [1]. To overcome this, several techniques have been developed, including radiator slot modifications to excite hybrid modes within the SIW cavity. For instance, dual-hybrid mode excitation has improved the FBW from 1.4% to 6.3%, along with moderate gain enhancement to 6.0 dBi [4]. Substrate slot removal has also been employed to reduce slot capacitance and widen bandwidth. This method yields a 24% improvement in FBW and a 6.2% increase in antenna efficiency, although it introduces fabrication complexity and retains single-resonant behavior [5]. This approach aims to widen the narrow bandwidth by minimizing the slot capacitance in the traditional cavity back slot (CBS) SIW antenna. Using this technique results in a 24% broader bandwidth and a 6.2% increase in antenna efficiency compared to the conventional CBS SIW design. However, removing the substrate is challenging, and although it broadens the impedance bandwidth, the antenna still resonates at a single frequency, limiting the overall improvement.

Another method for bandwidth enhancement, a design with dual unequal slot radiator modification was performed. The measurements demonstrated 420 MHz impedance bandwidth, which doubles that of the standard dual-slot antenna. Its appealing characteristics such as affordability, small footprint, and flat design facilitate straightforward integration into microwave planar circuits [6]. To achieve miniaturization, half-mode SIW (HMSIW) has been introduced, halving the antenna size but often at the cost of reduced bandwidth performance [7]. Redesigning the radiator using bow-tie slots enabled the generation of closely spaced hybrid modes, achieving a 1.03 GHz and a 3.7 dBi gain at X-band frequencies [8]. Placing the bow-tie-shaped slot at the cavity's top adjusts the loading effect, allowing for the optimization of slot dimensions to generate two closely spaced hybrid modes. These adjustments result in two resonances that significantly enhance bandwidth, contrasting sharply with the 1.7% bandwidth of a conventional slot antenna within an SIW cavity.

Slot geometry has continued to play a central role in bandwidth enhancement. Modified dumbbell slots have generated penta-resonant behavior, producing a wide bandwidth from 18.2 to 23.8 GHz at K-band frequencies [9]. However, this approach typically involves complex slot designs and higher fabrication precision, which may limit its practicality for compact or cost-sensitive applications. SIW CBS antenna design incorporates a hole above the slot to shorten its effective length, thereby creating additional resonances at higher frequencies. This modification enables the antenna to achieve an FBW that is 60% larger than a typical cavity-backed antenna [10]. Several SIW CBS designs have been reported, including a shorting-

* Corresponding author: Dian Widi Astuti (dian.widiastuti@mercubuana.ac.id).

vias slot achieving quad-resonance at X-band frequencies between 9.36 and 11.26 GHz [11], a cross-shaped design operating from 8.7 to 10.7 GHz [12], and an elliptical CBS covering 8.83–10.99 GHz [13]. These configurations demonstrated significant bandwidth broadening through the use of shorting vias. However, the implementation of such vias presents practical challenges due to the precision required in their placement.

Pin-loaded patches applied at C-band have achieved a 840 MHz bandwidth in the frequency range of 3.62–4.46 GHz, though they suffer from alignment complexity during fabrication [14]. Multi-resonant SIW antennas have also been proposed for hexa-band operation between 5 and 8 GHz, but each sub-band retains a narrow FBW, typically under 2% [15]. The antenna's cavity design incorporates simultaneous port relocation, multilevel patches, and additional vias to mitigate energy leakage between ports, thereby ensuring robust isolation (> 23.42 dB). The antenna produces six working frequencies, but the FBW value is very small at each frequency. The HMSIW CBS antenna with a single resonant frequency [16] has a narrow impedance bandwidth at S-band frequencies with an FBW value of 1.22%.

Several advanced structures, including quad-mode (QM) SIW and eight-mode (EM) SIW, have been implemented to support broader resonance across K-band, C-band, and S-band frequencies, with FBW values ranging from 7.7% to 13.2% [17, 18]. These studies operate in the K-band, C-band, and S-band frequency ranges, achieving FBW values of 7.7%, 13.2%, and 9.1%, respectively. SIWs with modified coupling [19, 20] however still produce relatively small FBWs at 10%, 16.2%, and 4.7%, respectively. The SIW antenna with metamaterial method [21] achieved bandwidth enhancement at C-band frequencies, exhibiting two distinct resonances and covering a frequency span of approximately 1.1 GHz. However, the integration of metamaterials often involves intricate design and fabrication processes. The SIW antenna with rectangular ring slots and long slits were engraved on the top surface of the antenna [22], working in two frequency ranges of S-band and C-band with FBW values of 0.7% and 5.5%, respectively. However, the FBW value obtained was still too small. The bandwidth improvement was achieved through the use of four resonant frequencies [23], which were generated within hybrid HMSIW cavities embedded between the inner and outer substrate layers. These cavities produced closely spaced frequency resonances. This approach is applied specifically to X-band frequencies using a low-profile substrate. Simulation results show an impedance bandwidth of approximately 3.66 GHz, spanning 8.98 to 12.64 GHz, with a peak gain of 7.97 dBi, while measured results indicate a bandwidth around 3.46 GHz, ranging from 9.14 to 12.6 GHz, and a peak gain of 7.62 dBi. Despite its high performance, this method relies on a multilayer structure and precise alignment between layers, which may complicate fabrication and limit scalability for compact or low-cost antenna systems.

Additionally, an HMSIW antenna utilizing a half-rectangular ring slot introduced a triple-resonant mechanism, yielding a measured bandwidth of approximately 3.38 GHz, operating from 7.89 to 11.27 GHz [24]. Similarly, modified I-shaped low-profile HMSIW antennas employing coplanar slot structures have achieved bandwidths greater than 1.85 GHz, covering the range of 8.7 to 10.55 GHz [25]. A wideband hexagonal SIW cavity-backed slot antenna array employing resonant and non-resonant slot combinations achieved an impedance bandwidth of approximately 1.5 GHz, with a measured peak gain of 12 dBi for the array configuration [26]. However, this design involves complex hexagonal geometries and requires precise alignment of multiple elements, which may increase fabrication difficulty and limit suitability for compact.

A half-mode SIW antenna integrated with a U-slot defected ground structure (DGS) achieved bandwidth enhancement of approximately 880 MHz, operating from 5.71 to 6.59 GHz through hybrid resonance of TE_{101} and TE_{102} modes [27]. However, the inclusion of both inner and outer HMSIW cavities, along with the DGS, increases design complexity and sensitivity to fabrication accuracy, which may limit its scalability for compact implementations. A broadband HMSIW antenna design employing a half-octagonal ring slot and outer cavity achieved a measured bandwidth of 1.25 GHz, covering 5.82–7.07 GHz, with a dual-resonant response formed by the merging of TE_{101} and TE_{102} modes [28]. However, the gain remains relatively moderate at 2.73 dBi, which may limit the antenna's applicability in scenarios requiring higher directivity or long-range communication. In this study, a novel approach is introduced using an inner half-mode SIW cavity featuring a half-octagonal ring slot to generate dual-resonant modes (TE_{101} and TE_{102}). These closely spaced resonances significantly enhance the impedance bandwidth. This design achieves a measured FBW of 5.6% in the S-band, with a 50% reduction in antenna size compared to conventional SIW configurations. The major contributions of this work are:

1. A new dual-resonant frequency excitation technique within an HMSIW cavity using a half-octagonal ring slot.
2. The impedance bandwidth improved to 5.6%, covering the frequency range of 3.15 to 3.33 GHz.
3. Maintenance of compact planar structure while preserving gain performance.
4. A significant miniaturization of 50% compared to traditional SIW designs.

2. ANTENNA DESIGN AND MATERIALS

The proposed antenna design, designated as Ant-C as shown in Fig. 1, employs an HMSIW configuration featuring an inner cavity embedded with a half-octagonal ring slot. The antenna is fabricated using a Rogers RT/Duroid 5880 substrate, characterized by a dielectric constant (ε_r) of 2.2, a loss tangent (δ) of 0.0009, and a substrate thickness of 1.575 mm. This configuration achieves a 50% size reduction compared to traditional full-mode SIW (FMSIW) structures while retaining essential wave-guiding properties. Simulations and design optimization were performed using ANSYS HFSS, and mode frequency predictions were based on classical SIW cavity theory [29, 30].

$$f_{mnp}^{SIW} = \frac{1}{2\pi\sqrt{\mu\varepsilon}}\sqrt{\left(\frac{m\pi}{L_{eff}^{SIW}}\right)^2 + \left(\frac{n\pi}{h}\right)^2 + \left(\frac{p\pi}{W_{eff}^{SIW}}\right)^2} \quad (1)$$

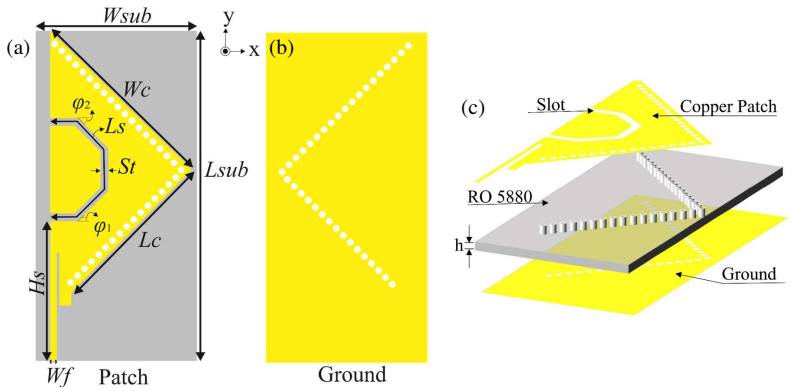

FIGURE 1. The design of Ant-C's HMSIW cavities include: (a) copper patch geometry, (b) ground plane specifics and (c) HMSIW 3D.

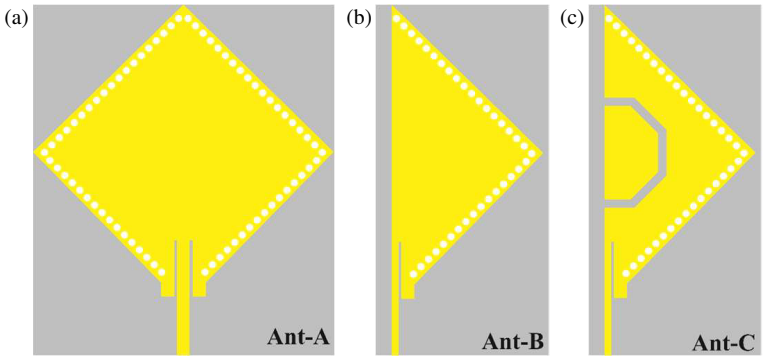

FIGURE 2. Evolution of HMSIW antenna, (a) basic cavity antenna with inner Ant-A, (b) HMSIW no slot Ant-B, (c) HMSIW with half-octagonal ring slot Ant-C.

where $m = 1, 2, ...$, $n = 1, 2$, $p = 1, 2, ...$ and $\mu = \mu_0 \cdot \mu_r$, $\varepsilon = \varepsilon_0 \cdot \varepsilon_r$ are the permeability and permittivity of the substrate, respectively. The thickness of the SIW resonator is h. The equivalent length and width (L_{eff}^{SIW} and W_{eff}^{SIW}) are as follows:

$$\begin{cases} L_{eff}^{SIW} = L_c - 1.08\,\frac{D_1^2}{V_3} + 0.1\,\frac{D_1^2}{L_c} \\ W_{eff}^{SIW} = W_c - 1.08\,\frac{D_1^2}{V_3} + 0.1\,\frac{D_1^2}{W_c} \end{cases} \tag{2}$$

$$\lambda_o = \frac{c}{f_c\sqrt{\varepsilon_r}} \tag{3}$$

The dimensions and specifications for Ant-C are presented in Table 1. The structure consists of a rectangular inner cavity modified with a half-octagonal ring slot etched into the top copper layer. This ring is composed of five segments: two horizontal, one vertical, and two diagonally slanted segments positioned at angles $\varphi_1 = -45°$ and $\varphi_2 = 45°$, respectively.

TABLE 1. Dimension of Ant-C (unit in millimeters).

Parameter	W_{sub}	L_{sub}	W_c	L_c	D_1
Value	61	125	53.5	53.5	2.5
Parameter	L_s	S_t	H_s	W_f	V_3
Value	64.2	3	52.94	2.425	3.75

The total slot length is approximately equal to the guided wavelength at the TE_{102} mode of the inner cavity. The slot excites dual resonant frequencies TE_{101} and TE_{102} allowing the antenna to achieve wider impedance bandwidth. The equivalent length and width of the resonator cavity are derived using classical waveguide theory, as shown in Equations (1)–(3). The antenna geometry is shown in Fig. 1, including the top copper patch, ground plane, and a 3D view of the HMSIW structure. The cavity dimensions were optimized to support operation in the S-band range, and the excitation of TE_{101} and TE_{102} modes is confirmed through simulation. The inner cavity is simultaneously fed with 50-ohm matched lines using quarter-wavelength transformers.

The antenna evolution is illustrated in Fig. 2. Ant-A represents the baseline FMSIW cavity design; Ant-B is the 50% miniaturized HMSIW structure without a slot; and Ant-C incorporates a half-octagonal ring slot. The slot perturbation in Ant-C leads to dual-mode excitation, resulting in a wider impedance bandwidth and more stable gain.

The TE modes of the FMSIW were analysed as illustrated in Fig. 3. The anticipated resonant frequencies corresponding to the TE_{101}, TE_{102}, TE_{202}, and TE_{103} modes occurred at frequencies of 2.08, 3.28, 4.17, and 4.67 GHz, respectively. These simulated results were consistent with the calculations shown in Table 2 [30]. TE mode simulations for the inner FMSIW cavity are summarized in Table 2 and visualized in Fig. 3. The narrowband nature and poor reflection coefficient of Ant-A are evident

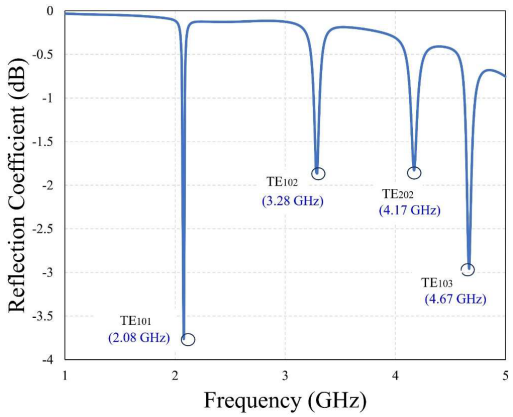

FIGURE 3. Simulation of the reflection coefficient for Ant-A's FMSIW.

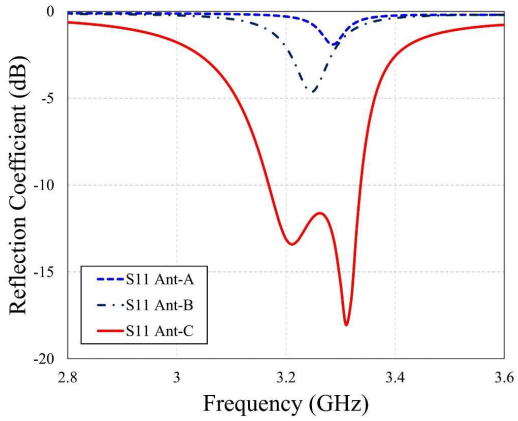

FIGURE 4. Simulated reflection coefficients for the progressive development of HMSIW cavity antennas.

TABLE 2. The calculated sequence of TE modes for the inner FMSIW cavities.

m\p	1	2	3	4	5
1	1.99	3.15	4.45	5.81	7.18
2		3.98	5.08	6.30	7.58
3				7.04	8.21
4				7.97	9.02
5					9.96

in Fig. 3. Fig. 4 presents the reflection coefficient improvements across Ant-B and Ant-C. The reflection coefficient evolution in Fig. 4 confirms that bandwidth broadening is achieved only in Ant-C.

The surface current distributions also affirm strong excitation of the slot at resonant frequencies. The implementation of the half-octagonal slot thus enables the merging of multiple TE modes, significantly improving bandwidth without sacrificing compactness.

Figure 5 demonstrates that Ant-C exhibits a consistently high and flatter realized gain profile, maintaining values above 5 dBi across the operational bandwidth of 3.17–3.34 GHz, with a peak gain of 5.47 dBi at 3.26 GHz. This enhancement is attributed to the dual-mode excitation of TE_{101} and TE_{102}, facilitated by the incorporation of the half-octagonal ring slot within the HMSIW cavity. Compared to Ant-A and Ant-B, which primarily operate in single-mode resonance, Ant-C achieves superior and more stable gain characteristics, while Ant-B reaches a slightly lower peak of 5.13 dBi at 3.8 GHz. The dual-resonance operation in Ant-C contributes to improved radiation performance and flatter gain response over the desired S-band frequency range.

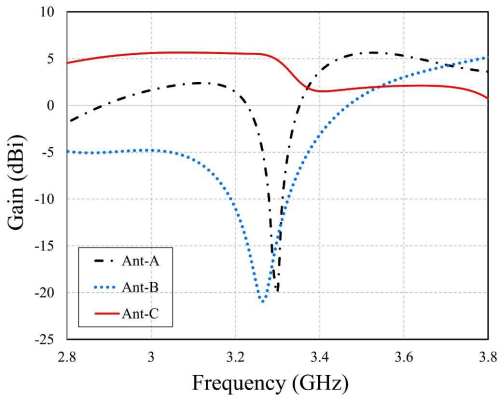

FIGURE 5. Peak realized gain of HMSIW.

3. METHODS AND PARAMETRIC STUDY

3.1. Electric Field Mode Analysis

The antenna was modelled based on actual physical parameters and boundary conditions. The simulation domain was configured with a radiation boundary and wave ports for realistic excitation and termination. A high-density mesh refinement was applied around the slot region, feedline, and cavity to improve numerical accuracy during parameter sweeps.

The electric field distribution (EFD) is analysed to examine the interaction of TE modes and their radiation behaviour into free space. Fig. 6 displays the EFD for Ant-A at 2.08 GHz. The EFD for Ant-A remains steady at 150 V/cm across one period for each 45° phase interval. In the observation of the simulated EFD at Ant-A in Fig. 6 there is a different electric distribution pattern from Fig. 7 observed at a frequency of 3.28 GHz, and the vector direction is also different when being observed with an internal phase of 45°.

Ant-C can produce dual resonant frequencies, resulting from combinations of the TE_{101} and TE_{102} modes. In Ant-C, the EFD is observed at 3.21 GHz, 3.26 GHz, and 3.31 GHz with phases 0°, 90°, 180°, and 270° as shown in Fig. 8. In Ant-C, the EFD is recorded at 150 V/cm per period, with measurements taken at 90° phase intervals. The EFD on Ant-C at 3.21 GHz arises from the interaction of the strong TE_{101} mode and weak TE_{102} mode combination. Fig. 8(a) illustrates the initial EFD at 3.21 GHz.

The highest electric field intensity within the inner HMSIW was observed along the horizontal, vertical, and both right and left slanted segments of the half-octagonal ring slot. Within the HMSIW structure, the field distribution arises from the combination of a dominant TE_{101} mode and a weaker TE_{102} mode occurring in-phase.

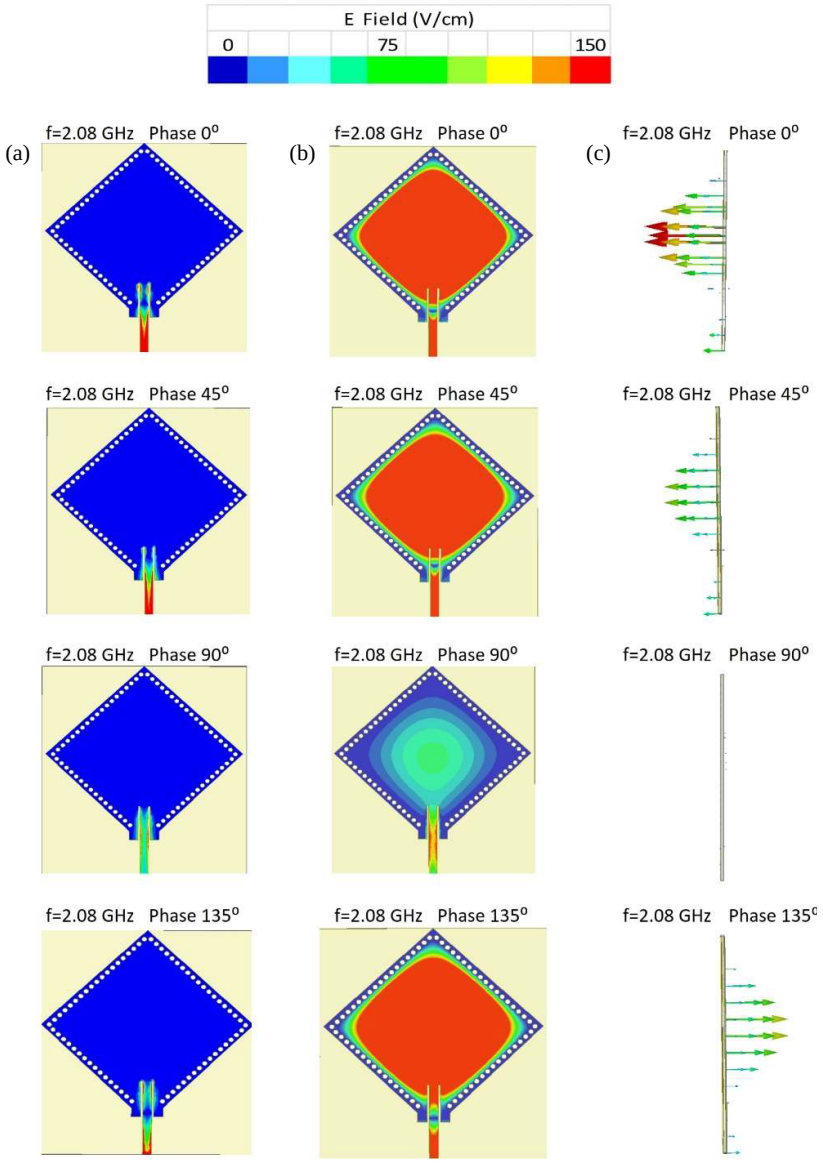

FIGURE 6. EFD of Ant-A at 2.08 GHz on phase 0°, 45°, 90° and 135°, (a) front patch, (b) back patch, (c) Vector E.

The second set of dual resonant frequencies appears at 3.31 GHz, as illustrated in Fig. 8(c). The highest EFD was found in the upper and lower sections of the half-octagonal ring slots within the inner HMSIW. At 3.31 GHz, the field distribution is produced by the interaction of a weaker TE_{101} mode and a stronger TE_{102} mode occurring out of phase. Additionally, significant distribution was observed in the feeding insert area of the HMSIW.

3.2. Parametric Analysis of Bandwidth enhancement

To understand the effect of the radiating slot's physical length (L_s) on bandwidth performance, a systematic parametric sweep was conducted while keeping other structural parameters fixed. The initial slot length was derived from the guided wavelength (λ_g) corresponding to the TE_{102} mode. The analysis indicated that shorter slot lengths weakened field interaction, while longer slots pushed upper-mode resonances outside the operating band. The slot was optimized to simultaneously excite TE_{101} and TE_{102} modes, enabling a broadened bandwidth configuration. The final chosen slot length offered optimal impedance matching and stable resonance behaviour across the S-band.

The slot thickness (S_t) was varied to evaluate its influence on the electromagnetic field behavior within the cavity. A thinner slot restricted field distribution, while excessive thickness resulted in the emergence of undesired parasitic modes. The optimal slot thickness enabled effective field interaction and supported stable dual-resonance operation, all while preserving the antenna's structural simplicity. This configuration proved essential for maintaining consistent performance across the desired frequency range.

Another key variable analysed was the vertical slot position (H_s) relative to the central axis of the HMSIW cavity. Centre-aligned slots supported strong TE_{101} excitation but limited interaction with higher-order modes. Asymmetrical placement

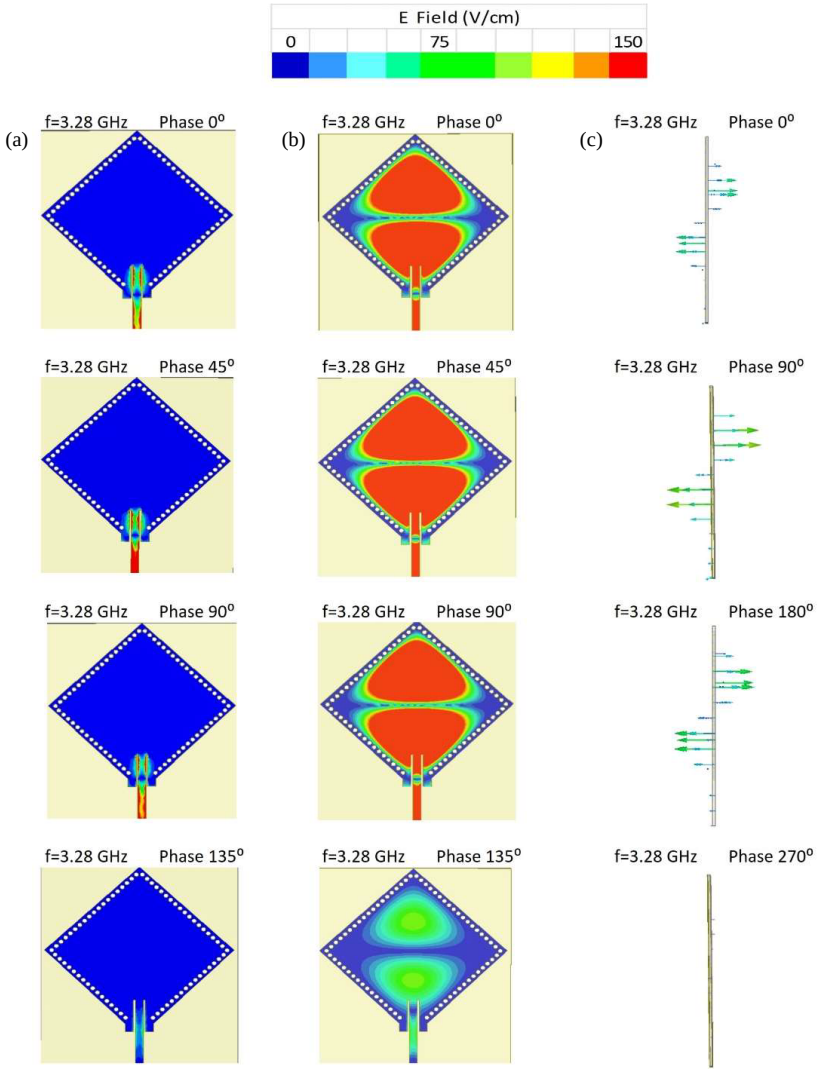

FIGURE 7. EFD of Ant-A at 3.28 GHz on phase 0°, 45°, 90° and 135°, (a) front patch, (b) back patch, (c) Vector E.

toward the top improved TE_{102} mode excitation. A suitable offset was identified that maximized the overlap between the two modes without introducing significant field distortion or degrading the radiation pattern.

4. RESULT AND DISCUSSION

The impact of varying the physical parameters of the radiating slot on the antenna's impedance bandwidth and mode behaviour was investigated using simulation analysis. The key results for slot length, thickness, and vertical position are summarized and discussed below.

The impact of the slot length (L_s) on the antenna's impedance bandwidth was evaluated through simulation, as presented in Fig. 9. The reference slot length was calculated based on the guided wavelength (λ_g) at the TE_{102} mode resonance, determined to be 64.85 mm using Formula (3). At this nominal length, the antenna achieved an FBW of 5.2%. To investigate sensitivity, the slot length was varied as a multiple of λ_g. When $L_s = 0.96\lambda_g$, the antenna exhibited a reduced FBW of 2.6%, with a narrow operational range between 3.08 and 3.16 GHz. Increasing the slot length to $1.03\lambda_g$ resulted in an FBW of 3.7%, extending the frequency range to 3.22–3.34 GHz. However, further extension to $1.09\lambda_g$ failed to maintain adequate impedance matching, as the reflection coefficient did not remain below -10 dB across the band. These results demonstrate that the optimal slot length lies close to the theoretical guided wavelength to enable effective dual-mode excitation and broad bandwidth performance.

The influence of the slot thickness S_t defined as the width of the half-octagonal ring slot was also investigated to determine its effect on bandwidth performance, as illustrated in Fig. 10. The optimal FBW was achieved when $S_t = 3.0$ mm, yielding a 5.2% bandwidth with effective dual-mode excitation. When the slot thickness was increased to 3.4 mm, the FBW slightly decreased to 4.6%, with the operational frequency range extending from 3.19 to 3.34 GHz. Reducing the slot thickness to 2.0 mm resulted in a further decrease in FBW to 2.9%, operating between 3.10 and 3.19 GHz. At the minimum tested thickness of 1.0 mm, the FBW was significantly reduced to 2.3%, with a narrow frequency range from 3.02 to 3.09 GHz. These findings indicate that slot thickness plays a critical role in field

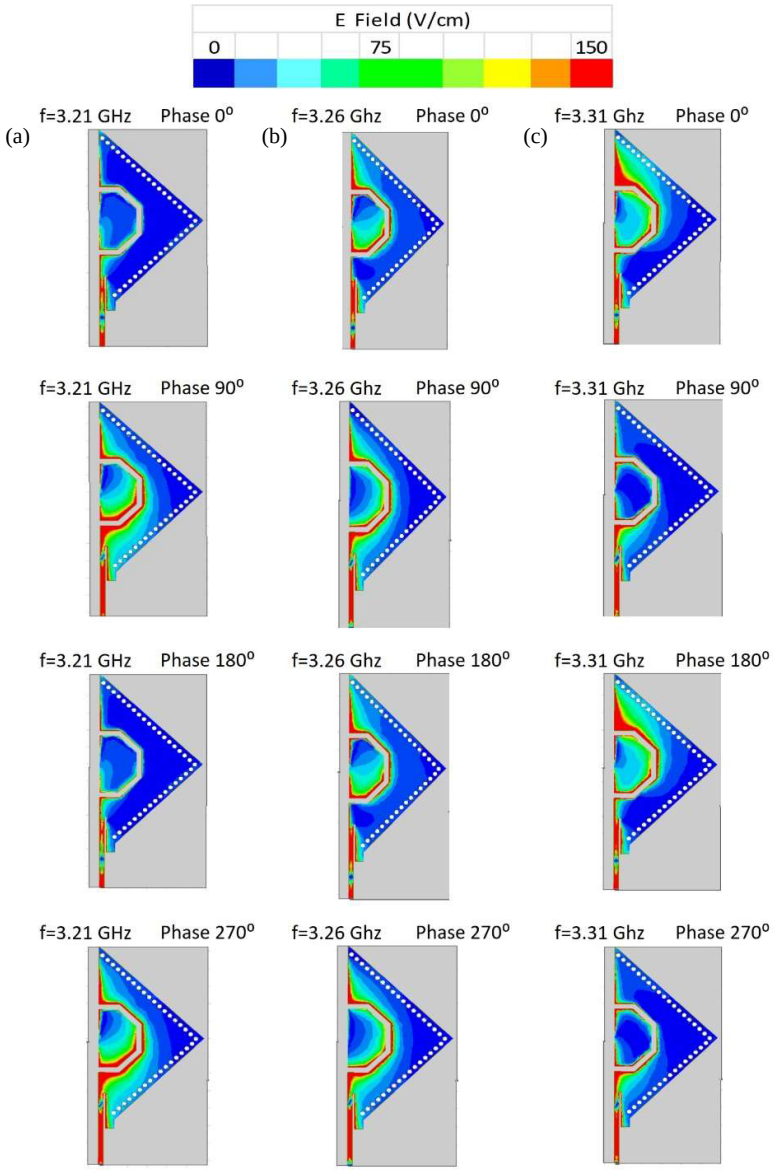

FIGURE 8. EFD of Ant-C at (a) 3.21 GHz, (b) 3.26 GHz, (c) 3.31 GHz on phase 0°, 90°, 180° and 270°.

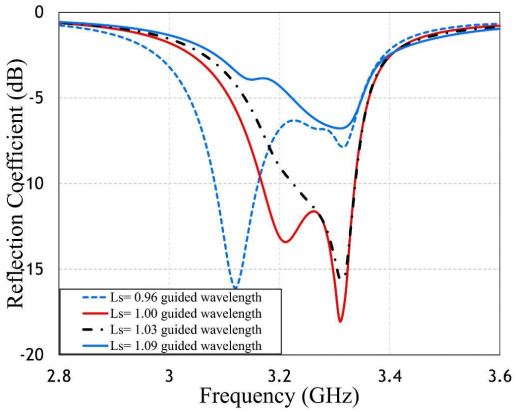

FIGURE 9. Simulated reflection coefficient for the L_s parameter, indicating the length of the half-octagonal ring slot.

coupling efficiency and that 3.0 mm offers an optimal trade-off between bandwidth broadening and mode stability.

The effect of the slot position H_s defined as the vertical distance from the feed point to the centre of the half-octagonal ring slot was analysed to determine its impact on impedance bandwidth. As shown in Fig. 11, the optimal configuration was found when $H_s = 52.94$ mm, which resulted in an FBW of 5.2%, covering the frequency range from 3.17 to 3.34 GHz. When the slot was slightly lowered to $H_s = 52.64$ mm, the FBW decreased to 3.1%, with an operating band from 3.17 to 3.27 GHz. Conversely, increasing the slot position to $H_s = 53.24$ mm further reduced the FBW to 1.2%, spanning 3.32 to 3.36 GHz. At the maximum tested position, $H_s = 53.54$ mm, the reflection coefficient failed to drop below -10 dB, indicating poor impedance matching and ineffective resonance. These results confirm that precise slot positioning is critical for achieving effective dual-mode excitation, and that $H_s =$

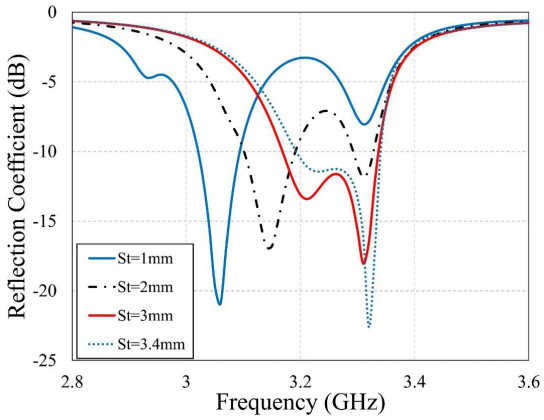

FIGURE 10. Simulated reflection coefficient for the S_t parameter, representing the thickness of the half-octagonal ring slot.

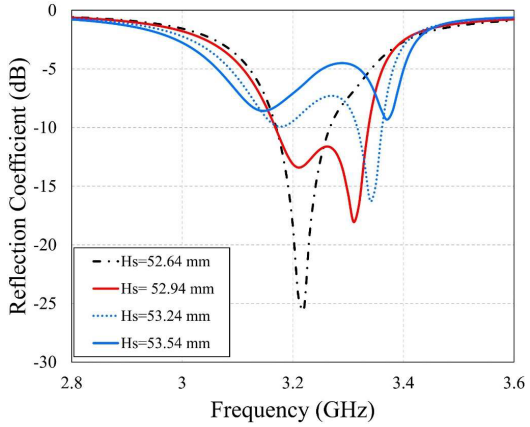

FIGURE 11. Simulated reflection coefficient for the H_s parameter, representing the position of the half-octagonal ring slot.

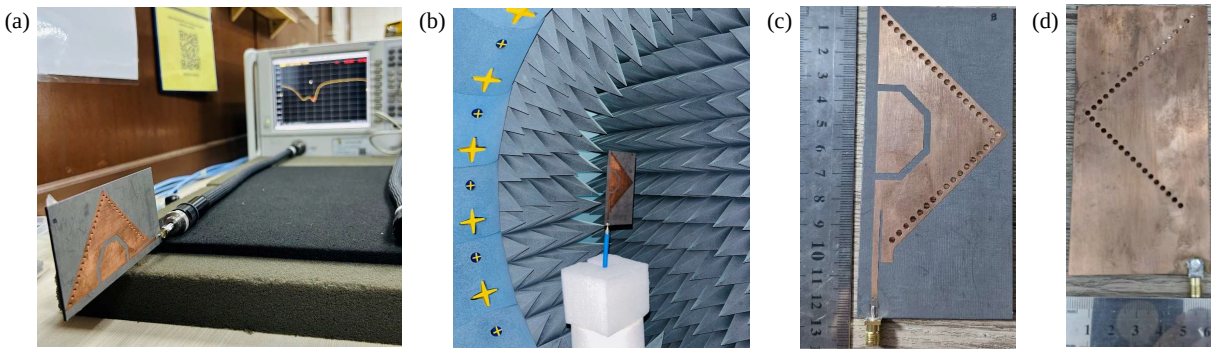

FIGURE 12. Fabricated antenna: (a) S_{11} measurement, (b) radiation pattern measurement, (c) patch view, (d) ground view.

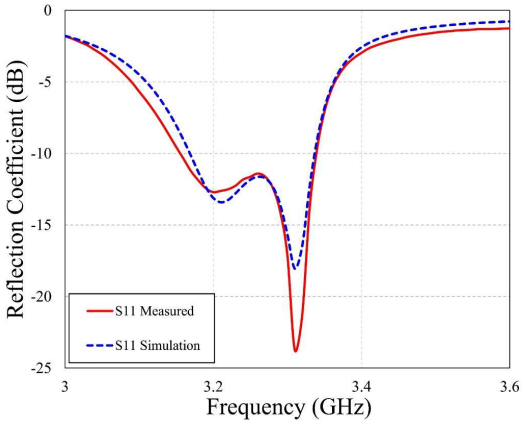

FIGURE 13. Simulation and measured reflection coefficients of the proposed antenna.

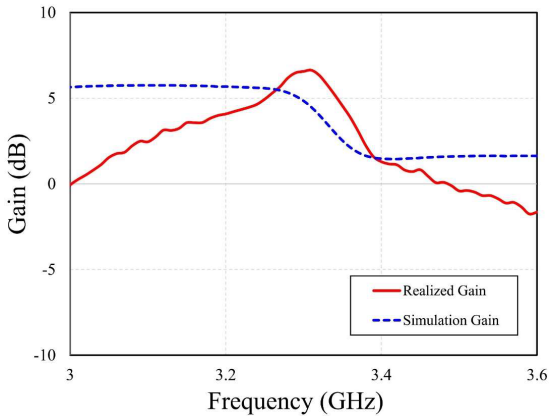

FIGURE 14. Realized and simulated gains of the proposed antenna.

52.94 mm provides the best alignment for broadband performance.

The fabricated antenna, shown in Fig. 12, was produced through a conventional photo etching technique The prototype was tested using a Vector Network Analyzer (VNA) to validate the simulated impedance bandwidth. As shown in Fig. 12(a), the measured reflection coefficient indicates that the antenna achieves a -10 dB impedance bandwidth of 180 MHz, corresponding to a frequency range of 3.15 to 3.33 GHz. This result closely aligns with the simulated bandwidth of 170 MHz, which spans 3.17 to 3.34 GHz. As illustrated in Fig. 13, the measured data exhibit minimal deviation from the simulation results. These minor discrepancies can be attributed to practical fabrication tolerances, variations in the placement of shorting vias, and potential inconsistencies in connector soldering. Despite these factors, the fabricated prototype confirms the antenna's capability to achieve broadband S-band performance with consistent impedance matching characteristics.

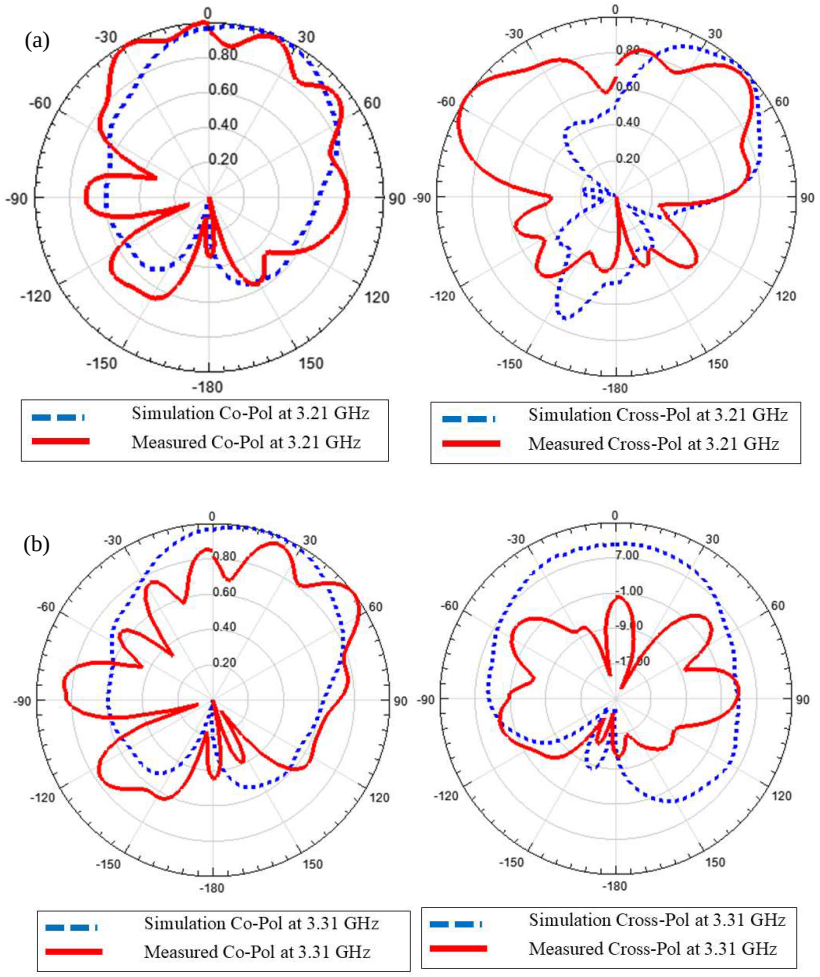

FIGURE 15. Simulation and measured radiation patterns at dual-resonant frequencies, (a) 3.21 GHz and (b) 3.31 GHz.

TABLE 3. Comparison of the proposed measured antenna with previously published research.

Ref.	Dimension (λ_o)	Gain Sim. dBi	F_c GHz	BW MHz	FBW %
[10]	$0.51 \times 0.45 \times 0.01$	5.8	2.45	82	3.3
[16]	$0.22 \times 0.34 \times 0.01$	4.12	2.45	30	1.22
[20]	$0.57 \times 0.54 \times 0.02$	5.74	3.4	160	4.7
[22]	$0.42 \times 0.42 \times 0.01$	2.37	2.41	18	0.75
This Work	$1.31 \times 0.64 \times 0.01$	5.6	3.24	180	5.6

The gain performance of the proposed antenna was analyzed through both simulation and measurement across the frequency range of 3–3.6 GHz, as illustrated in Fig. 14. The simulated gain exhibits a smooth and consistent trend, peaking at approximately 5.75 dBi within the operational band of 3.1–3.2 GHz, confirming the effective excitation of the TE_{101} and TE_{102} modes in the HMSIW cavity. The measured (realized) gain, although showing more fluctuation, gradually increases from negative values at lower frequencies and reaches a peak of approximately 6.63 dBi at 3.31 GHz, before tapering off at higher frequencies. The difference between simulated and measured gains is attributed to practical factors such as fabrication tolerance, connector losses, and measurement environment variations. Nevertheless, the overall consistency in peak gain and frequency behavior between the two datasets affirms the antenna's stable and directional radiation characteristics throughout the S-band frequency range.

Figure 15 presents the normalized radiation pattern of the proposed antenna based on both simulated and measured results at the dual resonant frequencies of 3.21 GHz and 3.31 GHz. The simulation was performed for the principal planes, specifically the E-plane ($\varphi = 0°$) and H-plane ($\varphi = 90°$), which correspond to the antenna's broadside and orthogonal directions, respectively. The results indicate a strong correlation between

simulation and measurement, particularly in the co-polarization patterns. Although the two planes exhibit similar directional characteristics, a minor deviation is detected in the main beam direction. This variation is attributed to electromagnetic interactions within the inner HMSIW cavity, specifically influenced by the EFD across the half-octagonal ring slot, as previously illustrated in Fig. 8.

Table 3 presents a comparative evaluation between the proposed antenna and previously reported designs in the literature. The integration of HMSIW cavities with dual-resonant frequencies in the proposed design has effectively enhanced the impedance bandwidth. The measured FBW reaches 5.6%, which exceeds the performance of many conventional SIW cavity-slot antennas operating in the S-band frequency range. While some earlier works achieved broader bandwidths, they typically involvef structurally complex solutions such as stacked substrates, shorting vias, or multilayer configurations. In contrast, the proposed antenna maintains a compact, single-layer structure, offering a favorable balance between electrical performance and fabrication simplicity.

5. CONCLUSION

In this paper, an HMSIW cavity antenna incorporating a half-octagonal ring slot has been designed, simulated, and experimentally validated to enhance impedance bandwidth for S-band applications. The integration of dual-resonant modes, TE_{101} and TE_{102}, within a compact HMSIW structure enabled the antenna to achieve a simulated fractional bandwidth of 5.2% (3.17–3.34 GHz) and a measured FBW of 5.6% (3.15–3.33 GHz), with consistent gain performance ranging from 3.1 dBi to 5.6 dBi and a directional radiation pattern. The proposed design achieves bandwidth enhancement using a single-layer cavity configuration, without requiring complex fabrication techniques such as multilayer stacking or shorting vias. This approach offers a practical and efficient solution for compact wireless systems operating in the S-band. The findings confirm that dual-mode excitation using a half-octagonal ring slot represents a valuable method for bandwidth improvement, with future potential in reconfigurable and multi-band antenna designs.

ACKNOWLEDGEMENT

Thank you to Direktorat Riset, Teknologi, dan Pengabdian Kepada Masyarakat (Kemdiktisaintek), Indonesia, which has funded this research under the Penelitian Tesis Mahasiswa scheme with the number 01-1-4/644/SPK/VII/2024 and Universiti Kebangsaan Malaysia for the supporting the antenna measurement.

REFERENCES

[1] Luo, G. Q., Z. F. Hu, L. X. Dong, and L. L. Sun, "Planar slot antenna backed by substrate integrated waveguide cavity," *IEEE Antennas and Wireless Propagation Letters*, Vol. 7, 236–239, 2008.

[2] Luo, G. Q., T. Y. Wang, and X. H. Zhang, "Review of low profile substrate integrated waveguide cavity backed antennas," *International Journal of Antennas and Propagation*, Vol. 2013, No. 1, 746920, 2013.

[3] Bozzi, M., A. Georgiadis, and K. Wu, "Review of substrate-integrated waveguide circuits and antennas," *IET Microwaves, Antennas & Propagation*, Vol. 5, No. 8, 909–920, Jun. 2011.

[4] Luo, G. Q., Z. F. Hu, W. J. Li, X. H. Zhang, L. L. Sun, and J. F. Zheng, "Bandwidth-enhanced low-profile cavity-backed slot antenna by using hybrid SIW cavity modes," *IEEE Transactions on Antennas and Propagation*, Vol. 60, No. 4, 1698–1704, 2012.

[5] Yun, S., D.-Y. Kim, and S. Nam, "Bandwidth and efficiency enhancement of cavity-backed slot antenna using a substrate removal," *IEEE Antennas and Wireless Propagation Letters*, Vol. 11, 1458–1461, 2012.

[6] Razavi, S. A. and M. H. Neshati, "Development of a linearly polarized cavity-backed antenna using HMSIW technique," *IEEE Antennas and Wireless Propagation Letters*, Vol. 11, 1307–1310, 2012.

[7] Mbaye, M., J. Hautcoeur, L. Talbi, and K. Hettak, "Bandwidth broadening of dual-slot antenna using substrate integrated waveguide (SIW)," *IEEE Antennas and Wireless Propagation Letters*, Vol. 12, 1169–1171, 2013.

[8] Mukherjee, S., A. Biswas, and K. V. Srivastava, "Broadband substrate integrated waveguide cavity-backed bow-tie slot antenna," *IEEE Antennas and Wireless Propagation Letters*, Vol. 13, 1152–1155, 2014.

[9] Cheng, T., W. Jiang, S. Gong, and Y. Yu, "Broadband SIW cavity-backed modified dumbbell-shaped slot antenna," *IEEE Antennas and Wireless Propagation Letters*, Vol. 18, No. 5, 936–940, 2019.

[10] Yun, S., D.-Y. Kim, and S. Nam, "Bandwidth enhancement of cavity-backed slot antenna using a via-hole above the slot," *IEEE Antennas and Wireless Propagation Letters*, Vol. 11, 1092–1095, 2012.

[11] Shi, Y., J. Liu, and Y. Long, "Wideband triple- and quad-resonance substrate integrated waveguide cavity-backed slot antennas with shorting vias," *IEEE Transactions on Antennas and Propagation*, Vol. 65, No. 11, 5768–5775, 2017.

[12] Wu, Q., J. Yin, C. Yu, H. Wang, and W. Hong, "Broadband planar SIW cavity-backed slot antennas aided by unbalanced shorting vias," *IEEE Antennas and Wireless Propagation Letters*, Vol. 18, No. 2, 363–367, 2019.

[13] Xiang, L., Y. Zhang, Y. Yu, and W. Hong, "Characterization and design of wideband penta- and hepta-resonance SIW elliptical cavity-backed slot antennas," *IEEE Access*, Vol. 8, 111 987–111 994, 2020.

[14] Zhang, X., T.-Y. Tan, Q.-S. Wu, L. Zhu, S. Zhong, and T. Yuan, "Pin-loaded patch antenna fed with a dual-mode SIW resonator for bandwidth enhancement and stable high gain," *IEEE Antennas and Wireless Propagation Letters*, Vol. 20, No. 2, 279–283, 2021.

[15] Dash, S. K. K., Q. S. Cheng, R. K. Barik, F. Jiang, N. C. Pradhan, and K. S. Subramanian, "A compact SIW cavity-backed self-multiplexing antenna for hexa-band operation," *IEEE Transactions on Antennas and Propagation*, Vol. 70, No. 3, 2283–2288, 2021.

[16] Astuti, D. W. and E. T. Rahardjo, "Size reduction of cavity backed slot antenna using half mode substrate integrated waveguide structure," in *2018 4th International Conference on Nano Electronics Research and Education (ICNERE)*, 1–4, Hamamatsu, Japan, Nov. 2018.

[17] Wu, Q., H. Wang, C. Yu, and W. Hong, "Low-profile circularly polarized cavity-backed antennas using SIW techniques," *IEEE Transactions on Antennas and Propagation*, Vol. 64, No. 7,

2832–2839, 2016.

[18] Chaturvedi, D., A. Kumar, and S. Raghavan, "Wideband HMSIW-based slotted antenna for wireless fidelity application," *IET Microwaves, Antennas & Propagation*, Vol. 13, No. 2, 258–262, 2019.

[19] Dashti, H. and M. H. Neshati, "Development of low-profile patch and semi-circular SIW cavity hybrid antennas," *IEEE Transactions on Antennas and Propagation*, Vol. 62, No. 9, 4481–4488, 2014.

[20] Zhou, J. and M. Yang, "A low-profile eighth-mode SIW antenna with dual-sense circular polarization, enhanced bandwidth and simple structure," *IEEE Access*, Vol. 9, 144 375–144 384, 2021.

[21] Caytan, O., S. Lemey, S. Agneessens, D. V. Ginste, P. Demeester, C. Loss, R. Salvado, and H. Rogier, "Half-mode substrate-integrated-waveguide cavity-backed slot antenna on cork substrate," *IEEE Antennas and Wireless Propagation Letters*, Vol. 15, 162–165, 2015.

[22] Qin, J., X. Fu, M. Sun, Q. Ren, and A. Chen, "Frequency reconfigurable antenna based on substrate integrated waveguide for S-band and C-band applications," *IEEE Access*, Vol. 9, 2839–2845, 2020.

[23] Astuti, D. W., Y. Wahyu, F. Y. Zulkifli, and E. T. Rahardjo, "Hybrid HMSIW cavities antenna with a half-pentagon ring slot for bandwidth enhancement," *IEEE Access*, Vol. 11, 18 417–18 426, 2023.

[24] Astuti, D. W., H. A. Majid, S. Alam, and A. Setyawan, "A broadband half-mode substrate integrated waveguide cavity antenna with triple-resonances," *Progress In Electromagnetics Research C*, Vol. 152, 55–66, 2025.

[25] Srinivas, L., G. A. Kumar, and G. Ram, "A novel design of modified I-shaped low profile broadband cavity-backed SIW slot antenna," *Journal of Electromagnetic Waves and Applications*, Vol. 38, No. 6, 724–737, 2024.

[26] Astuti, D. W., M. Muslim, U. Umaisaroh, H. A. Majid, S. Alam, and Y. Rahayu, "Broadband HMSIW antenna using a demi hexagonal ring slot for X-band application," *Sinergi (Indonesia)*, Vol. 29, No. 1, 73–82, 2025.

[27] Astuti, D. W., R. Rivayanto, M. Muslim, T. Firmansyah, D. A. Cahyasiwi, I. U. V. Simanjuntak, and Y. Natali, "Bandwidth enhancement for half mode substrate integrated waveguide antenna using defected ground structures," *International Journal of Electronics and Telecommunications*, Vol. 69, No. 3, 449–454, 2023.

[28] Setyawan, A., D. W. Astuti, M. Alaydrus, and Y. Wahyu, "Bandwidth enhancement of HMSIW antenna using half-octagonal ring slot," *J. Commun.*, Vol. 20, No. 2, 131–140, 2025.

[29] Jin, C., R. Li, A. Alphones, and X. Bao, "Quarter-mode substrate integrated waveguide and its application to antennas design," *IEEE Transactions on Antennas and Propagation*, Vol. 61, No. 6, 2921–2928, 2013.

[30] Pozar, D. M., *Microwave Engineering*, 4th ed., John Wiley & Sons, 2012.